



CHORUS

This is the accepted manuscript made available via CHORUS. The article has been published as:

Difference frequency generation of surface plasmon-polaritons in Landau quantized graphene

A. Ryan Kutayiah, Mikhail Tokman, Yongrui Wang, and Alexey Belyanin

Phys. Rev. B **98**, 115410 — Published 6 September 2018

DOI: [10.1103/PhysRevB.98.115410](https://doi.org/10.1103/PhysRevB.98.115410)

Difference frequency generation of surface plasmon-polaritons in Landau quantized graphene

A. Ryan Kutayiah,¹ Mikhail Tokman,² Yongrui Wang,¹ and Alexey Belyanin¹

¹*Department of Physics and Astronomy, Texas A&M University, College Station, TX, 77843 USA*

²*Institute of Applied Physics, Russian Academy of Sciences*

(Dated: August 9, 2018)

We develop a rigorous quantum-mechanical theory of the nonlinear optical process of difference frequency generation of surface plasmon-polaritons in Landau-quantized graphene. Although forbidden in the electric-dipole approximation, the second-order susceptibility is surprisingly high, equivalent to the bulk magnitude above 10^{-3} m/V. We consider the graphene monolayer as a nonlinear optical component of a monolithic photonic chip with integrated pump fields. The nonlinear power conversion efficiency of the order of tens $\mu\text{W}/\text{W}^2$ is predicted from structures of $10 - 100$ μm size. We investigate a variety of waveguide configurations to identify the optimal geometry for maximum efficiency.

I. INTRODUCTION

Many of the unique transport, thermal, and optical properties of graphene stem from the fact that its low-energy excitations are massless Dirac fermions [1]. Among its numerous applications is the use of graphene as an optoelectronic and plasmonic material. Graphene was shown to support highly-confined surface plasmon modes [2, 3]; it has relatively long-lived plasmon-polariton modes due to large intrinsic carrier mobilities and doping tunability [4–6], excellent electro-optic tunability [7], and large third-order and second-order optical nonlinearity [5, 10–13]. The latter is surprising since graphene is a centrosymmetric medium for low-energy in-plane excitations. Therefore, its in-plane second-order nonlinear response should be zero in the electric dipole approximation [14]. However, for obliquely incident or in-plane propagating electromagnetic (EM) fields, inversion symmetry is broken by nonzero wavevector components in the plane of graphene, and the second-order nonlinearity is nonzero and actually quite large [12, 13, 15–17]. It is enabled by effects of the spatial dispersion, or, in real space, by nonlocal effects beyond the electric dipole approximation. A particularly large value of $\chi^{(2)}$ equivalent to the bulk value of $\sim 10^{-3}$ m/V per monolayer [13] is reached at low frequencies, for the processes of frequency down-conversion to the terahertz range such as difference frequency generation (DFG) [12, 13, 18–20] or parametric down-conversion [16].

A strong magnetic field transverse to the graphene layer splits the continuous conical electron dispersion into a discrete set of non-equidistant Landau levels (LLs) [21]. The magnetic field does not break the inversion symmetry, so the DFG process remains forbidden in the electric dipole approximation. However, a strong magnetic field creates resonant transitions for all EM fields and enhances the electron density of states through the LL degeneracy. Both effects enhance optical nonlinearity [11, 22]. Further enhancement of the nonlinear generation efficiency is possible when the DFG sig-

nal is frequency- and phase-matched to surface plasmon-polaritons in graphene.

This work focuses on DFG in Landau-quantized graphene, particularly on the nonlinear generation of surface plasmon polaritons. In Section II we derive the dispersion equation for surface plasmon-polaritons in Landau-quantized graphene. In Section III We calculate the second-order nonlinear susceptibility and generated DFG signal power. For calculations of the Poynting flux of nonlinearly generated surface plasmon-polaritons, we focus on the monolithically integrated photonic chip geometry, including graphene as a nonlinear material and a dielectric waveguide or cavity with strong vertical confinement for the pump electromagnetic (EM) fields. We obtain analytic expressions for the DFG plasmon power and present its dependence on various parameters. We investigate a variety of waveguide configurations to identify the optimal geometry for maximum DFG efficiency. Our results can be easily extended to other (non-waveguide) geometries of the pump beams delivery and overlap.

II. DISPERSION OF SURFACE PLASMON-POLARITONS IN LANDAU-QUANTIZED GRAPHENE

We consider two possibilities for integrating a monolayer of graphene of area S into a dielectric waveguide or cavity; see Fig. 1a and Fig. 1b. There is a uniform magnetic field in the z -direction $\mathbf{B} = \mathbf{e}_z B$.

The dielectric constants of the waveguide layers ϵ_1 , ϵ_2 , and ϵ_3 will be taken as air, GaAs, and AlAs (respectively) or air, Si, and SiO₂ (respectively) for numerical examples below. However, many other combinations of the cladding and core layer materials are possible with the same qualitative results. The pump modes participating in the DFG are guided by the waveguide core ϵ_2 and are counterpropagating in the x -direction to provide phase matching to surface plasmon-polaritons (SPPs) supported by graphene at the difference frequency. This

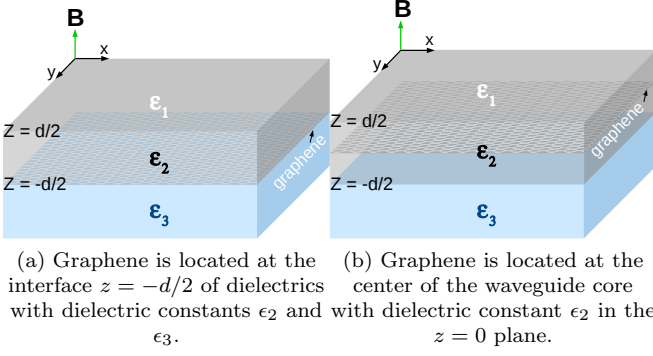


Figure 1. A sketch of integrated waveguide geometries.

arrangement ($\epsilon_1 \neq \epsilon_2 \neq \epsilon_3$) is what we refer to as the asymmetric waveguide. The special case where $\epsilon_1 = \epsilon_3$ (both are air) is what we will call the symmetric waveguide.

Note that the effect of disorder in adjacent dielectric layers can be detrimental for carrier mobility and optical transition linewidth in graphene. Many groups found it beneficial to encapsulate graphene between hexagonal boron nitride (hBN) layers. Early theoretical work indicated the possibility of opening the gap in graphene on hBN substrate [23], although subsequent experiments have not found any gap [24, 25]. This issue is not directly relevant to our study, so we will assume that graphene has an undistorted Dirac-cone electron dispersion at low energies and sufficiently high quality to have inter-LL transitions clearly resolved. We will neglect the thickness of dielectric hBN layers or any other encapsulating layers in the calculations of EM modes assuming that they are of nm thickness. They can be easily taken into account if needed.

A. Surface charge density for Landau-quantized graphene

The surface charge density for graphene in a magnetic field is given by

$$\rho(\mathbf{r}) = -e \sum_{\alpha, \beta} \rho_{\alpha\beta} \psi_{\beta}^*(\mathbf{r}) \psi_{\alpha}(\mathbf{r}) \quad (1)$$

where e is the elementary charge, $\rho_{\alpha\beta}$ is the density matrix, $\psi_{\alpha}(\mathbf{r})$ are the energy eigenstates for Landau-quantized graphene near the Dirac point as given in Appendix A, i.e. $\psi_{\alpha}(\mathbf{r}) = \psi_{nk}(\mathbf{r})$. They form a complete set and are orthonormal in the area S . The vector \mathbf{r} is in the graphene plane. The index α is a shorthand notation for electron quantum numbers n, k in a magnetic field.

Next we evaluate the spatial Fourier transform of the surface charge density,

$$\rho(\mathbf{r}) = \sum_q \rho_q e^{i\mathbf{q}\cdot\mathbf{r}}, \quad \rho_q = \frac{1}{S} \int d^2r e^{-i\mathbf{q}\cdot\mathbf{r}} \rho(\mathbf{r}), \quad (2)$$

where \mathbf{q} is in the plane of graphene. Substituting Eq. (1) into the integral in Eq. (2) gives

$$\rho_q = -\frac{e}{S} \sum_{\alpha, \beta} F_{\beta\alpha}(-\mathbf{q}) \rho_{\alpha\beta} \quad (3)$$

where $F_{\beta\alpha}(-\mathbf{q}) = \langle \beta | e^{-i\mathbf{q}\cdot\mathbf{r}} | \alpha \rangle$. Assuming that \mathbf{q} is directed along x , we obtain

$$\begin{aligned} F_{\beta\alpha}(-\mathbf{q}) &= \langle n, k' | e^{-iqx} | m, k \rangle \\ &= \langle n, k' | e^{-iqx} | m, k' + q \rangle \delta_{k, k'+q} \equiv \tilde{F}_{nk'm}(-q) \delta_{k, k'+q}. \end{aligned} \quad (4)$$

The matrix element $\tilde{F}_{nk'm}(-q)$ is calculated in Appendix B.

One needs to solve the density matrix equation for $\rho_{\alpha\beta}$ to obtain the Fourier component of the surface charge density ρ_q . We assume that the electric field of a graphene SPP in the plane of graphene is described by a scalar potential $\Phi(\mathbf{r}, t) = \text{Re}[\Phi_q e^{i\mathbf{q}\cdot\mathbf{r} - i\omega_q t}]$. The density matrix equation in the rotating wave approximation is

$$\begin{aligned} \dot{\rho}_{\alpha\beta} + \frac{i}{\hbar} (\mathcal{E}_{\alpha} - \mathcal{E}_{\beta}) \rho_{\alpha\beta} + \rho_{\alpha\beta} \gamma_{\alpha\beta} \\ = -\frac{i}{\hbar} (e\Phi_q e^{i\mathbf{q}\cdot\mathbf{r} - i\omega_q t})_{\alpha\beta} (f_{\alpha} - f_{\beta}) \end{aligned} \quad (5)$$

$$\implies \rho_{\alpha\beta}(t) = \frac{-eF_{\alpha\beta}(\mathbf{q})(f_{\alpha} - f_{\beta})}{\hbar(\omega_{\alpha\beta} - \omega_q - i\gamma_{\alpha\beta})} \Phi_q e^{-i\omega_q t}. \quad (6)$$

Here and below $\gamma_{\alpha\beta}$ is the phenomenological line broadening for a transition between states $|\alpha\rangle$ and $|\beta\rangle$, f_{α} is the occupation number of a given state. The line broadenings are determined by scattering on impurities and other disorder, electron-phonon scattering and electron-electron scattering. A rigorous treatment of scattering would require one to incorporate scattering rates for nonequilibrium carriers directly into the density matrix equations coupled with Maxwell's equations for all interacting fields. This will make the problem heavily numerical and this is far beyond the scope of this paper. Here we focus on the physical mechanism of DFG in a magnetized graphene and we keep the line broadenings as phenomenological parameters to obtain analytic expressions for the second-order nonlinear susceptibility and DFG efficiency. The scattering rates for Landau-quantized graphene were calculated e.g. in [26–28].

At high concentrations of nonequilibrium carriers the processes of electron-electron scattering and in particular resonant Auger scattering become important and even dominant in Landau-quantized graphene. As was shown in [28, 29], this can strongly affect the conditions for reaching inverted Landau-level distributions and lasing. However, in our case we assume that the Rabi frequencies of the pump fields are smaller than the carrier relaxation rate, so the optical population transfer is not important.

B. Dispersion relation for graphene surface plasmon-polaritons

The dispersion relation for SPPs in the quasi-electrostatic regime $q \gg \omega_q/c$ is obtained by using Gauss' law in 2D, the solution of the Laplace equation in a uniform dielectric (see also [12]),

$$(\epsilon_2 + \epsilon_3)q\Phi_q = 4\pi\rho_q, \quad (7)$$

and the relationship between the surface charge density and polarization, which is the definition of the surface linear susceptibility,

$$\rho_q = -q^2\chi_{\parallel}(\omega_q, \mathbf{q})\Phi_q. \quad (8)$$

The above two equations yield the dispersion relation

$$D(\omega_q, \mathbf{q}) = 1 + \frac{4\pi q}{\epsilon_2 + \epsilon_3}\chi_{\parallel}(\omega_q, \mathbf{q}) = 0. \quad (9)$$

Using Eqs. (3), (6), and (8) one arrives at the expression for the surface linear susceptibility,

$$\chi_{\parallel}(\omega_q, \mathbf{q}) = -\frac{e^2}{Sq^2} \sum_{\alpha, \beta} \frac{(f_{\alpha} - f_{\beta})|F_{\alpha\beta}(\mathbf{q})|^2}{\mathcal{E}_{\alpha} - \mathcal{E}_{\beta} - \hbar\omega_q - i\hbar\gamma_{\alpha\beta}}. \quad (10)$$

Inserting Eq. (10) into Eq. (9), results in the dispersion relation for a SPP in Landau-quantized graphene

$$D(\omega_q, \mathbf{q}) = 1 - \frac{4\pi e^2}{(\epsilon_2 + \epsilon_3)Sq} \sum_{\alpha, \beta} \frac{(f_{\alpha} - f_{\beta})|F_{\alpha\beta}(\mathbf{q})|^2}{\mathcal{E}_{\alpha} - \mathcal{E}_{\beta} - \hbar\omega_q - i\hbar\gamma_{\alpha\beta}}. \quad (11)$$

To avoid cumbersome expressions we consider resonant three-wave mixing when both pump modes and the difference frequency signal are resonant to three cascaded inter-LL transitions and form a closed loop, as shown in Fig. 2. Then it is enough to consider three Landau levels $| -n \rangle$, $| n-1 \rangle$, and $| n+1 \rangle$ which we relabel $| 1 \rangle$, $| 2 \rangle$, and $| 3 \rangle$, respectively. The pump fields at frequencies ω_1 and ω_2 are coupled to electric-dipole allowed transitions $| 1 \rangle \rightarrow | 3 \rangle$ and $| 1 \rangle \rightarrow | 2 \rangle$ which obey the selection rules $\Delta|n| = \pm 1$. However, the difference-frequency transition $| 2 \rangle \rightarrow | 3 \rangle$, or $| n-1 \rangle \rightarrow | n+1 \rangle$, does not and is therefore electric-dipole forbidden. This is another manifestation of the fact that DFG is electric-dipole-forbidden in monolayer graphene.

We assume for definiteness that the Fermi level is somewhere between states $| 2 \rangle$ and $| 3 \rangle$ but separated by more than $k_B T$ from state $| 3 \rangle$, see Fig. 2. The total degeneracy per Landau level scales as $\sim 10^{11} B \text{ cm}^{-2}$, where B is the magnetic field in Tesla. This means that for typical magnetic fields of a few Tesla assumed in the numerical estimates below the doping density required to fill the first two Landau levels does not exceed 10^{12} cm^{-2} . There should be no problem with achieving this level of doping.

The pump modes are TE-polarized and counterpropagating, in order to satisfy phase-matching conditions for a

DFG of SPPs. Their frequencies are resonant with transitions $| 1 \rangle \rightarrow | 3 \rangle$ and $| 1 \rangle \rightarrow | 2 \rangle$, respectively, i.e. $\omega_1 \approx \omega_{31}$ and $\omega_2 \approx \omega_{21}$.

Using the states given above and the fact that $f_{3k} \approx 0$ the dispersion relation (11) becomes

$$D(\omega_q, \mathbf{q}) = 1 + \frac{\omega_o(q)}{\omega_{32} - \omega_q - i\gamma_{32}} = 0 \quad (12)$$

where

$$\omega_o(q) = \frac{4\pi e^2(N_F/S)\xi(q)}{(\epsilon_2 + \epsilon_2)\hbar q}, \quad \xi(q) = \frac{\sum_k |\tilde{F}_{3k2}(q)|^2}{\kappa} \quad (13)$$

where $\kappa = 2S/\pi l_B^2$ is the Landau level degeneracy, $l_B = \sqrt{\hbar c/(eB)}$, $N_F = f_F \kappa$ is the number of particles in a completely filled Landau level, and $f_F = f_{2k'}$. It follows from Eq. (12) that

$$\text{Re}[\omega_q] = \omega_{32} + \omega_o(q), \quad \text{Im}[\omega_q] = -\gamma_{32}. \quad (14)$$

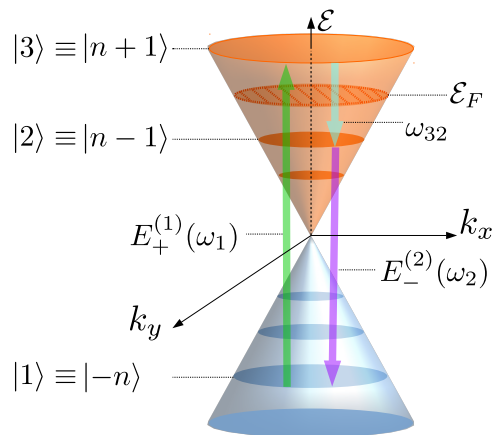


Figure 2. A sketch of Landau levels in graphene (not to scale) superimposed on the Dirac cone and the resonant DFG scheme. The pump fields E_{\pm} are coupled to electric-dipole allowed Landau level transitions. The difference frequency field is resonant to a dipole-forbidden transition.

For a dipole-forbidden transition $| 2 \rangle \rightarrow | 3 \rangle$ $|\tilde{F}_{3k2}(\mathbf{q})|^2 \propto q^{a>2}$ when q is small. For large q the quantity $|\tilde{F}_{3k2}(\mathbf{q})|^2$ goes to zero too.

III. DIFFERENCE-FREQUENCY GENERATION OF SPPS IN LANDAU-QUANTIZED GRAPHENE

A. Nonlinear charge density and second-order susceptibility

In the presence of the pump fields generating the polarization at the difference frequency, the surface charge density needs to be expanded to include nonlinear terms,

$$\rho_q = \rho_q^l + \rho_q^{nl}. \quad (15)$$

Here we identify the linear part as the one linearly proportional to the electric field, $\rho_q^l = -q^2 \chi_{\parallel}(\omega_q, \mathbf{q}) \phi_q$ (compare with Eq. (8)), where ϕ_q is the harmonic of the scalar potential of the SPP field and the nonlinear term as ρ_q^{nl} . By inserting Eq. (15) into Eq. (7) one can solve for ϕ_q in terms of the nonlinear part of the charge density ρ_q^{nl} ,

$$\phi_q = \frac{4\pi\rho_q^{nl}}{(\epsilon_2 + \epsilon_3)qD(\omega_q, \mathbf{q})}. \quad (16)$$

To derive the expression for the nonlinear charge density we express the Fourier component of the nonlinear surface charge density ρ_q^{nl} in terms of its matrix elements as done in Eq. (3). Following [30], we obtain the equation for the density matrix element $\rho_{3k2(k-q)}$, which corresponds to the transition $|3\rangle \rightarrow |2\rangle$,

$$\begin{aligned} \dot{\rho}_{3k2(k-q)} + i\omega_{32}\rho_{3k2(k-q)} + \gamma_{32}\rho_{3k2(k-q)} \\ = -i\frac{d_{21}^*E_-^{(2)*}(-d/2)e^{i\omega_2 t}}{\hbar}\rho_{3k1(k-q_1)}. \end{aligned} \quad (17)$$

Here and in all equations below the pump fields $E_+^{(1)*}, E_-^{(2)*}$ are taken on the graphene monolayer located at $z = -d/2$. Therefore, below we omit the argument $-d/2$ in the pump fields. Furthermore, $q = q_1 + q_2$, where $q_{1,2}$ are the projections of wavevectors of the optical fields on the graphene plane.

We see that the density matrix for the transition $|3\rangle \rightarrow |2\rangle$ depends on the linear perturbation of the matrix element for the transition $|3\rangle \rightarrow |1\rangle$. There is no contribution from the density matrix for the transition $|2\rangle \rightarrow |1\rangle$ because states $|1\rangle$ and $|2\rangle$ are below the Fermi level and assumed fully occupied. Consequently, the difference in their population is zero. We will assume that the pump field is not strong enough to cause significant population transfer, which means that its Rabi frequency should be smaller than the electron relaxation rate. On the other hand, we do keep a resonant Fourier harmonic of the nonlinear density perturbation in Eq. (15) which has a frequency and wave number equal to those for the surface plasmon wave, i.e. the one which matches the dispersion relation of a surface plasmon. It is this component which is responsible for the DFG effect.

The density matrix element for the $|3\rangle \rightarrow |1\rangle$ transition in Eq. (17) can be solved within the electric dipole approximation,

$$\begin{aligned} \dot{\rho}_{3k1(k-q_1)} + i\omega_{31}\rho_{3k1(k-q_1)} + \gamma_{31}\rho_{3k1(k-q_1)} \\ = i\frac{d_{31}E_+^{(1)}e^{-i\omega_1 t}}{\hbar}f_F, \end{aligned} \quad (18)$$

$$\text{or } \rho_{3k1(k-q_1)}(t) = \frac{e^{-i\omega_1 t}f_F}{\omega_{31} - \omega_1 - i\gamma_{31}}\frac{d_{31}E_+^{(1)}}{\hbar}. \quad (19)$$

Inserting Eq. (19) into Eq. (17) yields:

$$\begin{aligned} \rho_{3k2(k-q)}(t) = -\frac{e^{-i(\omega_1 - \omega_2)t}f_F}{(\omega_{32} - (\omega_1 - \omega_2) - i\gamma_{32})(\omega_{31} - \omega_1 - i\gamma_{31})} \\ \times \frac{d_{31}d_{21}^*E_+^{(1)}E_-^{(2)*}}{\hbar^2}. \end{aligned} \quad (20)$$

We are now equipped with almost all the pieces to express the amplitude of the SPP field in terms of the pump field amplitudes. The last piece of information we need is the expression for ρ_q^{nl} which is obtained from Eqs. (3), (4), and (20),

$$\begin{aligned} \rho_q^{nl}(t) = \frac{(N_F/S)\zeta(q)e^{-i\omega_d t}}{(\omega_{32} - \omega_d - i\gamma_{32})(\omega_{31} - \omega_1 - i\gamma_{31})} \\ \times \frac{ed_{31}d_{21}^*E_+^{(1)}E_-^{(2)*}}{\hbar^2}, \end{aligned} \quad (21)$$

where $\omega_d = \omega_1 - \omega_2$, and $\zeta(q) = \sum_{k'} \tilde{F}_{2k'3}(-\mathbf{q})/\kappa$. The matrix elements entering the expression for $\zeta(q)$ are evaluated in Appendix B.

Note that the second-order nonlinear susceptibility $\chi^{(2)}$ can be extracted from Eq. (21) by using $\rho_q^{nl} = -i\mathbf{q} \cdot \mathbf{P}_q^{nl} = -iq\chi^{(2)}E_+E_-^*$:

$$\chi^{(2)}(\omega_q, \mathbf{q}) = \frac{i}{q} \frac{(N_F/S)\zeta(q)}{(\omega_{32} - \omega_d - i\gamma_{32})(\omega_{31} - \omega_1 - i\gamma_{31})} \frac{ed_{31}d_{21}^*}{\hbar^2}. \quad (22)$$

As shown in Appendix B, one can derive an analytic expression for the matrix element $\zeta(q)$ for any set of three LLs participating in a three-wave mixing process. The resulting analytic expression for $\chi^{(2)}$ gives explicit dependence on all relevant parameters. For example, when the LL numbers involved in a resonant DFG process are -3, 2, and 4, and the $n = 2$ Landau level is completely occupied, the factor $(N_F/S)\zeta(q)$ in Eq. (22) is approximately equal to $0.235q^2$, where we used Eq. (B10) obtained in the limit $l_B q \ll 1$. The latter is valid since $q = q_1 + q_2$ scales as $(v_F/c)(1/l_B)$ times a numerical factor of the order of 10. Therefore, the magnitude of $\chi^{(2)}$ scales linearly with q .

Furthermore, the dipole moments of the pump transitions are roughly $ev_F/\omega_{1,2} \propto el_B$, so the peak value of $\chi^{(2)}$ scales as $1/\sqrt{B}$: $|\chi^{(2)}| \propto \frac{v_F}{c} \frac{e^3 l_B}{\hbar^2 \gamma_{31} \gamma_{21}}$ at resonance.

For $B = 1$ T, $|\chi^{(2)}| \simeq 2 \times 10^{-7}$ in CGS units. If the line broadening is dominated by impurity scattering, the scattering rates $\gamma_{21,31} \propto \sqrt{B}$ [26, 27] and $|\chi^{(2)}|$ scales as $1/B^{3/2}$.

Note that Eq. (22) looks ‘‘almost’’ like an expression for the second-order susceptibility of a three-level medium with 2D density given by the total degeneracy per Landau level, $2/(\pi l_B^2)$. An important difference is an extra factor $ql_B \ll 1$. This small factor is due to the fact that second-order processes are forbidden in graphene in the electric-dipole approximation. Just for the sake

of comparison with nonlinear crystals, we can divide by graphene monolayer thickness to get the ‘‘bulk’’ magnitude of $|\chi_{3D}^{(2)}| \sim 3 \times 10^{-3}$ m/V, which is a very large number. Of course the resulting DFG power depends on the magnitude of the surface (2D) $\chi^{(2)}$, as well as the overlap of modes with graphene and the sample size.

Finally, the expression of the field amplitude of the SPP mode can be obtained by substituting Eq. (21) into Eq. (16),

$$\phi_q = \frac{4\pi}{(\epsilon_2 + \epsilon_3)qD(\omega_q, \mathbf{q})} \times \frac{ed_{31}d_{21}^*E_+^{(1)}E_-^{(2)*}(N_F/S)\zeta(q)}{\hbar^2(\omega_{32} - \omega_d - i\gamma_{32})(\omega_{31} - \omega_1 - i\gamma_{31})}. \quad (23)$$

After making use of Eq. (12) and some straightforward manipulations one arrives at the final expression for the Fourier harmonic of the scalar potential of the SPP field:

$$\phi_q = \frac{4\pi e(N_F/S)\zeta(q)}{(\epsilon_2 + \epsilon_3)q} \times \frac{(d_{31}d_{21}^*E_+^{(1)}E_-^{(2)*})/\hbar^2}{(\omega_{32} + \omega_0(q) - (\omega_1 - \omega_2) - i\gamma_{32})(\omega_{31} - \omega_1 - i\gamma_{31})}. \quad (24)$$

As is clear from Eq. (24), the excitation of the SPP mode at frequency ω_q given by Eq. (14) is most efficient when the difference frequency $\omega_d = \omega_1 - \omega_2$ of the two-color pump field is in resonance with ω_q , i.e. $\omega_d = \omega_q$.

B. Poynting Flux in a SPP Mode

In the quasi-electrostatic approximation the time derivative of the magnetic field of the electromagnetic wave is negligible. In order to calculate the Poynting flux of the transverse magnetic (TM) SPP mode we need to go beyond the quasi-electrostatic approximation. Using Maxwell’s equations (see also [12]), we derive all required components of the electric and magnetic fields starting from the tangential component of the electric field, that is, the field along the x -axis of the graphene monolayer:

$$E_{xq}(z = -d/2) \equiv E_{xq}^o = -iq\phi_q; \quad (25)$$

$$E_x(x, z, t) = E_{xq}^o e^{iqx - i\omega_q t} \begin{cases} e^{-p_2(z+d/2)} & z > -d/2 \\ e^{+p_3(z+d/2)} & z < -d/2 \end{cases}, \quad (26)$$

$$E_z(x, z, t) = \pm \frac{iq}{p_{2,3}} E_x(x, z, t), \quad (27)$$

$$B_y(x, z, t) = \mp \frac{i\omega_q \epsilon_{2,3}}{cp_{2,3}} E_z(x, z, t), \quad (28)$$

where $p_{2,3} = \sqrt{q^2 - \epsilon_{2,3}\omega_q^2/c^2} > 0$ is the inverse confinement length in the z -direction. In \pm or \mp the top

sign corresponds to $z > -d/2$ and the bottom sign corresponds to $z < -d/2$.

The Poynting flux is then

$$\mathbf{S} = \frac{c}{8\pi} (\mathbf{E} \times \mathbf{B}^*) \quad (29)$$

$$= \mathbf{e}_x \frac{\omega_q q^3}{8\pi} |\phi_q|^2 \begin{cases} \frac{\epsilon_2}{p_2^2} e^{-2p_2(z+d/2)}, & z > -d/2 \\ \frac{\epsilon_3}{p_3^2} e^{+2p_3(z+d/2)}, & z < -d/2 \end{cases} \quad (30)$$

To calculate the power in the SPP mode at the difference frequency, we integrate the Poynting flux Eq. (29) over the differential area $\mathbf{e}_x dy dz \rightarrow \mathbf{e}_x L_y dz$, assuming that a graphene sample is uniform in the y -direction. The power is then

$$P_{DFG} = \frac{L_y \omega_q q^3 |\phi_q|^2}{16\pi} \left(\frac{\epsilon_2}{p_2^2} + \frac{\epsilon_3}{p_3^2} \right). \quad (31)$$

In the approximation $q \gg \omega_q/c$ we can write $p_{2,3} \approx q$, $q^3(\epsilon_2/p_2^2 + \epsilon_3/p_3^2) \approx \epsilon_2 + \epsilon_3$. Using this approximation along with Eq. (24) gives the final expression for the SPP power:

$$P_{DFG} = \frac{\pi L_y (\omega_1 - \omega_2)}{\epsilon_2 + \epsilon_3} \left[\frac{e(N_F/S)}{q} \right]^2 \times \left| \frac{(d_{31}d_{21}^*E_+^{(1)}E_-^{(2)*})/\hbar^2 \zeta(q)}{(\omega_{32} + \omega_0(q) - (\omega_1 - \omega_2) - i\gamma_{32})(\omega_{31} - \omega_1 - i\gamma_{31})} \right|^2. \quad (32)$$

This expression was derived for the graphene monolayer at the interface of the dielectric waveguide core and cladding. Similar formulas can be obtained for any other location of graphene.

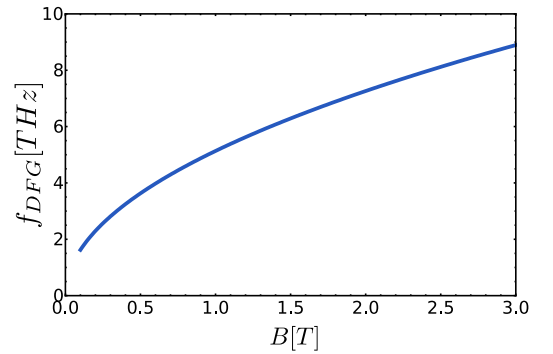


Figure 3. The DFG frequency resonant to the transition between Landau-level numbers 2 and 4 as a function of the magnetic field strength.

Figures 4-6 illustrate the dependence of the DFG power on various parameters for different waveguide compositions and locations of the graphene monolayer. The structure width L_y is chosen to be 100 μm . The power scales linearly with L_y . For the plots we choose the initial state |1> in Fig. 2 to have the Landau level index

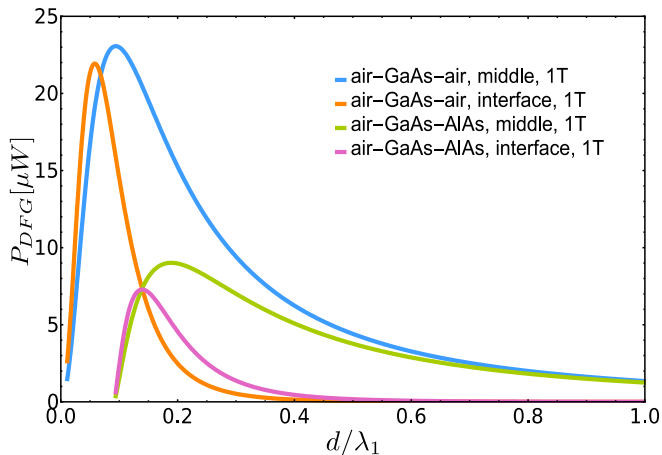


Figure 4. DFG power per 1 W^2 of the pump power as a function of the waveguide core thickness for the magnetic field strength 1T. In the legend of the plot “middle” means that graphene is in the middle of the core dielectric ϵ_2 ; “interface” means that graphene is located at the interface of dielectrics ϵ_2 and ϵ_3 . “1T” and “3T” stands for 1 and 3 Tesla magnetic field.

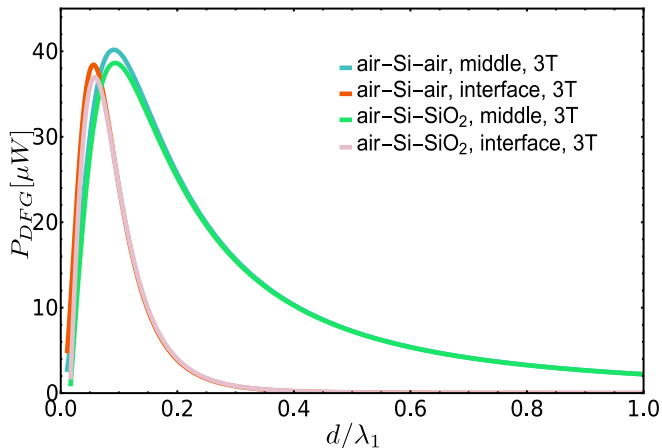


Figure 5. DFG power per 1 W^2 as a function of core thickness for the magnetic field strength 3 T. A higher magnetic field is chosen to avoid THz absorption in Si.

$n = -3$. Then the states $|2\rangle$ and $|3\rangle$ coupled to state $|1\rangle$ by electric dipole-allowed pump transitions have Landau level numbers $|n| - 1 = 2$ and $|n| + 1 = 4$, respectively. The DFG frequency corresponding to the transition between these states is in the THz range; see Fig. 3. The pump wavelengths are in the mid-infrared; for example, at $B = 1 \text{ T}$ they are $10.9 \mu\text{m}$ and $9.1 \mu\text{m}$. All frequencies scale as \sqrt{B} . The pump powers are assumed to be 1 W each, so that the plots actually show DFG power conversion efficiency in $\mu\text{W}/\text{W}^2$.

Figures 4 and 5 show the dependence of the DFG power on the thickness of the waveguide core for differ-

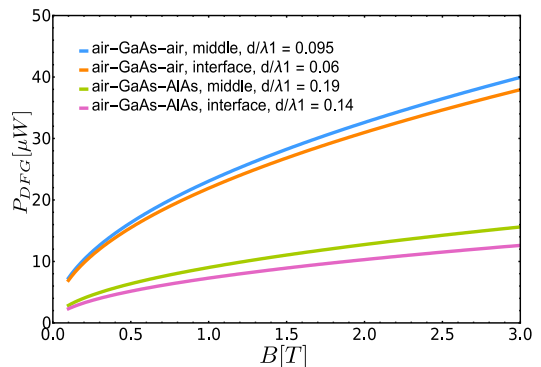


Figure 6. The DFG power per 1 W^2 as a function of the magnetic field for several waveguide structures and geometries. In the legend of the plot “middle” means that graphene is in the middle of the core dielectric ϵ_2 ; “interface” means that graphene is located at the interface of dielectrics ϵ_2 and ϵ_3 .

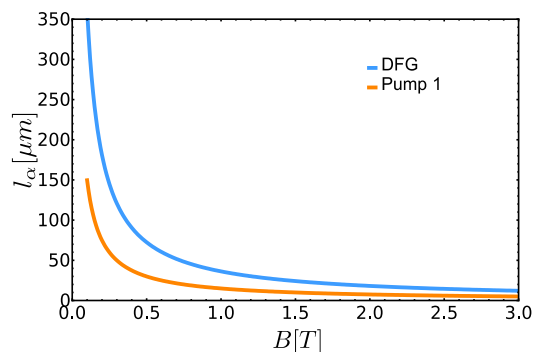


Figure 7. Absorption length for pump field intensity and DFG plasmon-polaritons as a function of the magnetic field for a symmetric GaAs waveguide with graphene at the interface. The core thickness is $0.06\lambda_1$.

ent positions of the graphene sheet and different waveguide materials at a fixed magnetic field. The DFG power depends on the magnitude of the in-plane components of the pump fields on graphene and the localization of the optical pump power. There is an optimal waveguide thickness which maximizes the DFG power for a given total power in the pump fields. For wider waveguide cores the in-plane component of the pump field amplitude on graphene gets smaller, whereas for narrower waveguides the pump field mode gets delocalized. Figures 4 and 5 also indicate that it is beneficial to place graphene in the middle of the waveguide core.

With increasing magnetic field the peak DFG power in Eq. (31) scales as \sqrt{B} , provided the pump wavelengths are tuned in resonance with corresponding transitions. This dependence is illustrated in Fig. 6 for a particular choice of waveguide structures and geometries. Note that the choice of particular pump and DFG transitions for a given magnetic field is strongly influenced by absorption

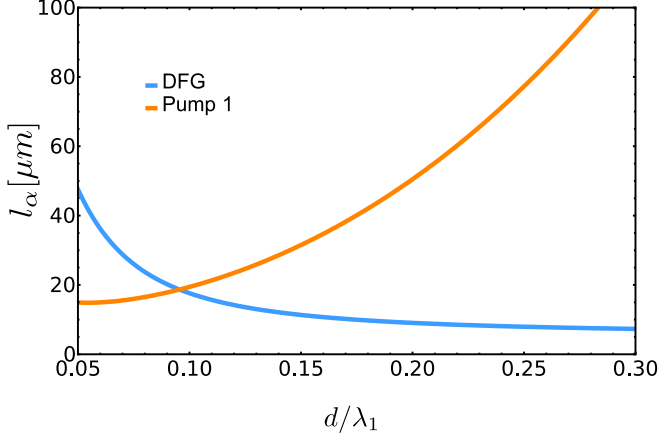


Figure 8. Absorption length for pump field intensity and DFG plasmon-polaritons as a function of core thickness for a symmetric GaAs waveguide with graphene at the interface. The magnetic field is 1T.

in the waveguide materials. For example, one should obviously avoid reststrahlen bands in all waveguide layers.

The DFG power can be further enhanced by stacking several monolayers together. However, there is a trade-off between the nonlinear conversion efficiency and absorption in graphene. We calculated the absorption of both pump and difference frequency modes.

The simplest way to calculate the absorption of the SPP mode is to solve its dispersion equation Eq. (12) for a complex wavenumber q as a function of a real frequency ω , i.e. as a boundary-value problem. Then the absorption length of the plasmon field intensity is

$$l_{\text{abs}} = \frac{1}{2} \text{Im}q \simeq \frac{1}{2} \gamma_{32} \left(\frac{\partial[\omega_o(q)]}{\partial q} \right)^{-1}, \quad (33)$$

assuming $|\text{Im}q| \ll |\text{Re}q|$.

Among the two pump fields, the strongest absorption is experienced by the one at frequency ω_1 resonant with transition $|1\rangle \rightarrow |3\rangle$, because state $|1\rangle$ is below the Fermi level whereas state $|3\rangle$ is above the Fermi level. Its absorption length can be found from the linear conductivity calculated in Appendix D and the Poynting flux calculated in Appendix C:

$$\frac{1}{l_{\text{abs}}(\omega_1)} = \frac{1}{8} \frac{\text{Re}[\sigma^{+-}(\omega_1)] |E_y^{(1)}(z = -d/2)|^2}{\langle \Phi_S^{(1)} \rangle}. \quad (34)$$

The dependence of the absorption length from the magnetic field and the waveguide core thickness is shown in Figs. 7 and 8, assuming exact resonance with corresponding LL transitions and the linewidth of 10^{12} s^{-1} . This is a rather small linewidth corresponding to a high-quality graphene encapsulated in hBN. Therefore we probably overestimate the absorption rate for most samples and the actual absorption length is longer. In any

case, for structures longer than the pump absorption length the pump field mode should be excited by a beam coupled from the top rather than from the facet, in order to reduce the propagation length.

In conclusion, we investigated an electric-dipole-forbidden process of THz difference frequency generation in Landau-quantized graphene. The second-order susceptibility turned out to be surprisingly high, equivalent to the bulk magnitude of about $3 \times 10^{-3} \text{ m/V}$. We applied the formalism to the DFG of THz surface plasmon-polaritons in graphene integrated into a dielectric waveguide or cavity with strong vertical confinement of the optical pump modes. The DFG power conversion efficiency of the order of tens $\mu\text{W}/\text{W}^2$ is predicted from structures of size around $100 \mu\text{m}$. Analytic expressions for the DFG power are obtained and the results are presented for different structure geometries, composition, and magnetic field strengths. Other three-wave mixing processes in a Landau-quantized graphene, such as sum-frequency generation or parametric down-conversion can be analyzed following the same approach.

IV. ACKNOWLEDGEMENT

This material is based upon work supported by the Air Force Office of Scientific Research under award number FA9550-17-1-0341. M.T. acknowledges the support from RFBR grant No. 17-02-00387.

Appendix A: Eigenstates, optical matrix elements, and selection rules for Landau-quantized graphene

For graphene in a constant external magnetic field $\mathbf{p} \rightarrow \boldsymbol{\pi} = \mathbf{p} + e\mathbf{A}/c$, where \mathbf{p} is the canonical momentum, $\boldsymbol{\pi}$ is the gauge-invariant kinetic momentum and \mathbf{A} is the vector potential that generates the magnetic field $\mathbf{B} = \nabla \times \mathbf{A}$. The effective mass low-energy Hamiltonian (neglecting the spin degree of freedom) is then [21]

$$H_{\Xi}^B = \Xi v_F \boldsymbol{\sigma} \cdot \boldsymbol{\pi}, \quad (A1)$$

where $\boldsymbol{\sigma}$ is the vector of Pauli matrices and $\Xi = \pm 1$ depending on the valley. Assuming that the magnetic field $\mathbf{B} = \mathbf{e}_z B$ is perpendicular to the plane of the graphene sheet and using the Landau gauge $\mathbf{A} = -\mathbf{e}_x y B$, the eigenfunctions [32] are

$$\psi_{nk}^K(\mathbf{r}) = \frac{C_n}{\sqrt{L}} e^{ikx} \begin{pmatrix} \text{sgn}(n) i^{|n|-1} \phi_{|n|-1,k}(y) \\ i^{|n|} \phi_{|n|,k}(y) \\ 0 \\ 0 \end{pmatrix} \quad (A2)$$

and

$$\psi_{nk}^{K'}(\mathbf{r}) = \frac{C_n}{\sqrt{L}} e^{ikx} \begin{pmatrix} 0 \\ 0 \\ i^{|n|} \phi_{|n|,k}(y) \\ \text{sgn}(n) i^{|n|-1} \phi_{|n|-1,k}(y) \end{pmatrix} \quad (A3)$$

where

$$\phi_{|n|,k}(y) = \frac{H_{|n|}((y - kl_B^2)/l_B)}{\sqrt{2^{|n|}|n|!}\sqrt{\pi}l_B} \exp\left[-\frac{1}{2}\left(\frac{y - kl_B^2}{l_B}\right)^2\right] \quad (\text{A4})$$

with energy eigenvalue [32, 33]

$$\mathcal{E}_n = \text{sgn}(n)\hbar\omega_c\sqrt{|n|}; \quad (\text{A5})$$

L^2 is the area of the system, $n = 0, \pm 1, \pm 2, \dots$ is the Landau level index, $\omega_c = \sqrt{2}v_F/l_B$ is the cyclotron frequency, $l_B = \sqrt{c\hbar/eB}$ is the magnetic length, $H_{|n|}((y - kl_B^2)/l_B)$ are the Hermite polynomials, $C_n = 1$ for $n = 0$ and $1/2$ otherwise. Henceforth, all calculations will be carried out using the effective mass low-energy Hamiltonian (A1) in the vicinity of the K point ($\Xi = +1$) and its eigenfunctions (A2).

The Hamiltonian for graphene in a magnetic field and an optical field is [11, 34]

$$H = H^B + H^{opt} = v_F\boldsymbol{\sigma} \cdot \boldsymbol{\pi} + v_F\boldsymbol{\sigma} \cdot \frac{e\mathbf{A}^{opt}(t)}{c} \quad (\text{A6})$$

H^{opt} is the interaction Hamiltonian.

Note that the wavefunction (A2) can be written as $\psi_{n,k}(\mathbf{r}) = \langle \mathbf{r} | n, k \rangle$. We'll make use of the state ket for graphene in a magnetic field $|n, k\rangle$ which will at times be written as $|\alpha\rangle$ for convenience.

We utilize the notation above in calculating the optical matrix element for transitions between the LLs resonant with the optical field (in the electric dipole approximation)

$$\langle n, k' | H^{opt} | m, k \rangle = v_F \frac{e\mathbf{A}^{opt}(t)}{c} \cdot \langle n, k' | \boldsymbol{\sigma} | m, k \rangle. \quad (\text{A7})$$

It is convenient to change to the circular polarization basis $\mathbf{e}_\pm \equiv 1/\sqrt{2}(\mathbf{e}_x \pm i\mathbf{e}_y)$, termed left-circularly polarized (LCP) and right-circularly polarized (RCP), respectively. The following relations holds true: $\mathbf{e}_\pm \cdot \mathbf{e}_\pm = 0$ and $\mathbf{e}_\pm \cdot \mathbf{e}_\mp = 1$. In the \mathbf{e}_\pm basis $Re[\mathbf{A}^{opt}] = c/i\omega_{opt}(\mathbf{e}_+E_+(t) + \mathbf{e}_-E_-(t)) + c.c.$, where $E_\pm(t) = 1/\sqrt{2}((E_x/2) \mp i(E_y/2))e^{-i\omega_{opt}t}$. Similarly, the vector of Pauli matrices in the \mathbf{e}_\pm basis is $\boldsymbol{\sigma} = \mathbf{e}_+\sigma^+ + \mathbf{e}_-\sigma^-$ where

$$\sigma^+ = \begin{pmatrix} 0 & 0 \\ \sqrt{2} & 0 \end{pmatrix}, \quad \sigma^- = \begin{pmatrix} 0 & \sqrt{2} \\ 0 & 0 \end{pmatrix}. \quad (\text{A8})$$

For a transition between Landau levels m and n resonant with the optical field ($\omega_{nm} \approx \omega_{opt} \equiv \omega$) we obtain

$$\begin{aligned} \langle n, k' | H^{opt} | m, k \rangle &= \delta_{kk'}\sqrt{2}v_FC_nC_m(\mathbf{e}_-\text{sgn}(n)\delta_{|n|-1,|m|} \\ &+ \mathbf{e}_+\text{sgn}(m)\delta_{|n|+1,|m|}) \cdot \left(e \frac{\mathbf{e}_+E_+(t) + \mathbf{e}_-E_-(t)}{i\omega} + c.c. \right) \\ \langle n, k' | H^{opt} | m, k \rangle &= \delta_{kk'} \frac{\sqrt{2}v_FeC_nC_m}{i\omega} \times \\ &(\text{sgn}(n)E_+(t)\delta_{|n|-1,|m|} + \text{sgn}(m)E_-(t)\delta_{|n|+1,|m|}) + c.c. \end{aligned} \quad (\text{A9})$$

Equation (A9) gives the selection rules for optical transitions between adjacent Landau levels i.e. $\Delta|m| = \pm 1$ [22, 34–36]. Furthermore, the transition $|m| \rightarrow |n| \pm 1$ couples to the RCP/LCP component of the optical field, respectively. From Eq. (A9) one also obtains the magnitude of the dipole moment [37]

$$|d_{nm}| = \sqrt{2}C_nC_m \frac{ev_F}{\omega}. \quad (\text{A10})$$

Appendix B: Calculation of the matrix element $F_{nkmk'}(\mathbf{q})$

Using the wavefunctions Eq. (A2) with Eq. (A4) the matrix element $F_{nkmk'}(\mathbf{q})$ can be calculated as

$$F_{nkmk'}(\mathbf{q}) = \langle n, k | e^{iqx} | m, k' \rangle \quad (\text{B1})$$

$$\begin{aligned} F_{nkmk'}(\mathbf{q}) &= \frac{C_nC_m}{L} \int dx e^{i(k'-(k-q))x} \\ &\times \int dy \left(\text{sgn}(n)i^{-|n|+1}\phi_{|n|-1,k}(y), i^{-|n|}\phi_{|n|,k}(y) \right) \\ &\times \left(\text{sgn}(m)i^{|m|-1}\phi_{|m|-1,k'}(y) \right) \\ &\times \left(i^{|m|}\phi_{|m|,k'}(y) \right) \\ F_{nkmk'} &= \frac{C_nC_m}{L} L\delta_{k',k-q}i^{|m|-|n|} \\ &\times \int dy [\text{sgn}(n)\text{sgn}(m)\phi_{|n|-1,k}(y) \times \phi_{|m|-1,k-q}(y) \\ &+ \phi_{|n|,k}(y) \times \phi_{|m|,k-q}(y)] \\ F_{nkmk'} &= C_nC_m i^{|m|-|n|}\delta_{k',k-q}[\text{sgn}(n)\text{sgn}(m) \\ &\times \langle \phi_{|n|-1,k} | \phi_{|m|-1,k-q} \rangle + \langle \phi_{|n|,k} | \phi_{|m|,k-q} \rangle]. \end{aligned} \quad (\text{B2})$$

Here

$$\int dx e^{i(k'-(k-q))x} = L\delta_{k',k-q}. \quad (\text{B3})$$

Introducing the notation

$$F_{nkmk'} = \tilde{F}_{nkm}\delta_{k',k-q} \quad (\text{B4})$$

and comparing equations (B2) and (B4) we see that

$$\begin{aligned} \tilde{F}_{nkm} &= C_nC_m i^{|m|-|n|}[\text{sgn}(n)\text{sgn}(m) \\ &\times \langle \phi_{|n|-1,k} | \phi_{|m|-1,k-q} \rangle + \langle \phi_{|n|,k} | \phi_{|m|,k-q} \rangle]. \end{aligned} \quad (\text{B5})$$

We also have

$$\text{sgn}(n)\text{sgn}(m) = \begin{cases} +1 & \text{intra-band transitions} \\ -1 & \text{inter-band transitions} \end{cases}. \quad (\text{B6})$$

In the main text we have the states labeled in the following way: $|1\rangle = |-|m|\rangle$, $|2\rangle = ||m|-1\rangle$, $|3\rangle = ||m|+1\rangle$. With this labeling, the second-order nonlinear susceptibility and the corresponding SPP field contain the matrix element $F_{3k2k'} = \tilde{F}_{3k2}\delta_{k',k-q}$. So for the initial state of

$m \neq 0$ we have

$$\begin{aligned}
& F_{3k2k'} \rightarrow \\
& F_{|m|+1,k,|m|-1,k'} = \delta_{k',k-q} C_{|m|+1} C_{|m|-1} i^{|m|-1-(|m|+1)} \\
& \times [\langle \phi_{|m|+1-1,k} | \phi_{|m|-1-1,k-q} \rangle + \langle \phi_{|m|+1,k} | \phi_{|m|-1,k-q} \rangle] \\
& F_{3k2k'} \rightarrow F_{|m|+1,k,|m|-1,k'} = -\delta_{k',k-q} C_{|m|+1} C_{|m|-1} \\
& \times [\langle \phi_{|m|,k} | \phi_{|m|-2,k-q} \rangle + \langle \phi_{|m|+1,k} | \phi_{|m|-1,k-q} \rangle] \quad (\text{B7})
\end{aligned}$$

For the initial state $m = -3$ we have

$$\begin{aligned}
& F_{|m|+1,k,|m|-1,k'} \rightarrow \\
& F_{4k2k'} = -\frac{1}{2} \delta_{k',k-q} [\langle \phi_{3,k} | \phi_{1,k-q} \rangle + \langle \phi_{4,k} | \phi_{2,k-q} \rangle] \\
& \tilde{F}_{4k2} = -\frac{1}{2} [\langle \phi_{3,k} | \phi_{1,k-q} \rangle + \langle \phi_{4,k} | \phi_{2,k-q} \rangle] \quad (\text{B8})
\end{aligned}$$

The analytic expression for \tilde{F}_{4k2} is

$$\begin{aligned}
& \tilde{F}_{4k2}(q) = - \left[\frac{24(2 + \sqrt{2}) - 4(4 + \sqrt{2})l_B^2 q^2 + l_B^4 q^4}{128\sqrt{3}} \right] \\
& \times l_B^2 q^2 e^{-(l_B^2 q^2/4)} \quad (\text{B9})
\end{aligned}$$

$$\tilde{F}_{4k2}(q) \approx - \left[\frac{24(2 + \sqrt{2})}{128\sqrt{3}} \right] l_B^2 q^2, \quad (\text{B10})$$

where in the last expression we assumed that $l_B q \ll 1$. This is always a good approximation since $q = q_1 + q_2$ scales as $(v_F/c)(1/l_B)$ times a number of the order of 10, if the LL numbers involved in the DFG process are not too high: around 2-4.

The factor $\zeta(q)$ in the main text is defined as follows:

$$\zeta(q) = \frac{1}{\kappa} \sum_{k'} \tilde{F}_{2k'4}(-q) \quad (\text{B11})$$

where $\kappa = 2S/\pi l_B^2$ and $l_B = \sqrt{\hbar/eB}$. From Eq. (B9) we see that $\tilde{F}_{2k'4}(-q)$ is independent of k' and can be taken out of the sum. Next we use:

$$\sum_{k'} \rightarrow 4L_x L_y / 2\pi l_B^2 = \kappa \quad (\text{B12})$$

using Eq. (B12) in Eq. (B11) we find

$$\zeta(q) = \tilde{F}_{4k'2}^*(q) \propto l_B^2 \propto 1/B. \quad (\text{B13})$$

Appendix C: Normalization of pump fields

We begin by considering the waveguide structure where the interfaces are at $z = d/2$ and $z = -d/2$. The thickness of the core layer is d and a monolayer of graphene is located at the interface $z = -d/2$. The dielectric constant is then:

$$\epsilon_j = \begin{cases} \epsilon_1 & z > d/2 \\ \epsilon_2 & -d/2 < z < d/2 \\ \epsilon_3 & z < -d/2. \end{cases} \quad (\text{C1})$$

We have two counter propagating TE polarized pump fields in the waveguide $\mathbf{E}^{1,2}(x, z, t) = \text{Re}[(0, E_y^{1,2}(z), 0)e^{\pm i q_1, 2 x - i \omega_{1, 2} t}]$.

Both pump fields obey the wave equation (in each region of the waveguide indexed by j):

$$(\nabla^2 - \frac{\epsilon_j}{c^2} \partial_t^2) \mathbf{E}_j^l(x, z, t) = 0 \quad (\text{C2})$$

$$\Rightarrow \frac{d^2 E_{jy}^l(z)}{dz^2} = \lambda_{jl} E_{jy}^l(z). \quad (\text{C3})$$

Here the eigenvalue determining the confinement of the pump field to the core layer of the waveguide is

$$\lambda_{jl} = \begin{cases} +\kappa_{1l}^2 & z > d/2 \\ -\alpha_l^2 & -d/2 < z < d/2 \\ +\kappa_{3l}^2 & z < -d/2 \end{cases} \quad (\text{C4})$$

where

$$\kappa_{(1,3)l} = \sqrt{q_l^2 - \epsilon_{1,3} \frac{\omega_l^2}{c^2}} \quad (\text{C5})$$

$$\alpha_l = \sqrt{\epsilon_2 \frac{\omega_l^2}{c^2} - q_l^2} \quad (\text{C6})$$

with the confinement condition $n_{1,3} < n_{eff} < n_2$ where $n_j^2 \approx \epsilon_j$ for small losses. The solution to the eigenvalue equation (C3) along with the continuity of the tangential component $E_{jy}(z)$ of the pump fields at interfaces $z = \pm d/2$ gives:

$$E_{jy}^l(z) = A_l f_{jl}(z) \quad (\text{C7})$$

$$f_{jl}(z) = \begin{cases} \cos(\alpha_l d/2 - \phi_l) e^{-\kappa_{1l}(z-d/2)} & z > d/2 \\ \cos(\alpha_l z - \phi_l) & -d/2 < z < d/2 \\ (\cos(\alpha_l d/2 + \phi_l) e^{\kappa_{3l}(z+d/2)}) & z < -d/2 \end{cases} \quad (\text{C8})$$

We will drop the index j for derivations that follow while keeping in mind that the field profile $f_{jl}(z)$ is a piecewise function. Next we find the amplitude A by normalizing the average Poynting flux $\langle \Phi_S \rangle$ to 1 W. We will drop the superscript l of the fields.

Let \mathbf{F} represent \mathbf{E} and \mathbf{B} . We can write the field $\mathbf{F} = \text{Re}[\mathbf{F}_R e^{-i\omega t}] = \frac{1}{2}(\mathbf{F}_R e^{-i\omega t} + \mathbf{F}_R^* e^{i\omega t})$, where $\mathbf{F}_R = \mathbf{F}_o e^{i\mathbf{k}\cdot\mathbf{r}}$. For a TE polarized field $\mathbf{E}_R = (0, E_y(z), 0)e^{iqx}$, $\mathbf{B}_R = (B_x(z), 0, B_z(z))e^{iqx}$. The time average of the Poynting flux is:

$$\langle \Phi_S \rangle = \frac{c}{8\pi} \int d\mathbf{A} \cdot \text{Re}[\mathbf{E}_R \times \mathbf{B}_R^*] \quad (\text{C9})$$

or, for the pumps propagating along the x-direction,

$$\langle \Phi_S \rangle = \frac{c}{8\pi} \int dy dz \text{Re}[E_y(x, z) B_z^*(x, z)] \quad (\text{C10})$$

We will assume that the fields are uniform along y , so integration over y results in multiplying by the length of the waveguide in the y -direction, L_y .

From Maxwell equations for a TE mode

$$B_z^*(x, z) = \frac{cq}{\omega} E_y^*(x, z). \quad (\text{C11})$$

The Poynting flux for TE pump fields is therefore

$$\langle \Phi_S^l \rangle = \frac{q_l L_y c^2}{8\pi\omega_l} \int_{-\infty}^{\infty} dz |E_y^l(z)|^2 \quad (\text{C12})$$

Finally, we normalize the Poynting flux $\langle \Phi_S \rangle$ as $\langle \Phi_S \rangle = P_o$, where P_o is the input pump power. This gives

$$A_l = \sqrt{\frac{P_o}{\frac{q_l L_y c^2}{8\pi\omega_l} F_l}} \quad (\text{C13})$$

where

$$F_l = \int_{-\infty}^{\infty} dz |f_l(z)|^2. \quad (\text{C14})$$

Appendix D: Linear conductivity of Landau-quantized graphene

Linear conductivity of Landau-quantized graphene has been calculated a number of times before. Here we summarize one approach to the derivation, which is based on the density matrix equation where the Hamiltonian is given by Eq. (A6),

$$\begin{aligned} \dot{\rho}_{\alpha\beta} &= \frac{i}{\hbar} [\rho, H]_{\alpha\beta} - \gamma_{\alpha\beta} \rho_{\alpha\beta} \\ &= \frac{i}{\hbar} (H_{\beta\beta} - H_{\alpha\alpha}) \rho_{\alpha\beta} + \frac{i}{\hbar} (\rho_{\alpha\alpha} - \rho_{\beta\beta}) H_{\alpha\beta} - \gamma_{\alpha\beta} \rho_{\alpha\beta} \end{aligned} \quad (\text{D1})$$

$\rho_{\alpha\beta}$ is the density matrix element, $\gamma_{\alpha\beta}$ is the phenomenological decay term. The states $|\alpha\rangle$ are eigen-states of the Hamiltonian H^B , i.e. $H^B |\alpha\rangle = \mathcal{E}_\alpha |\alpha\rangle$. In the dipole approximation (D1) becomes:

$$\begin{aligned} \dot{\rho}_{\alpha\beta}(t) &= i(-\omega_{\alpha\beta} + i\gamma_{\alpha\beta}) \rho_{\alpha\beta}(t) - \frac{1}{i\hbar} (f_\alpha - f_\beta) \\ &\times e v_F \boldsymbol{\sigma}_{\alpha\beta} \cdot \left(\frac{\mathbf{E}}{i\omega_l} e^{-i\omega_l t} + c.c. \right) \end{aligned} \quad (\text{D2})$$

where $f_\alpha = \rho_{\alpha\alpha}$ is 1 if the state $|\alpha\rangle$ is occupied or 0 if it's unoccupied; $\omega_{\alpha\beta} = (\mathcal{E}_\alpha - \mathcal{E}_\beta)/\hbar$, $\mathbf{E} = \mathbf{e}_+ E_+ + \mathbf{e}_- E_-$. In the rotating wave approximation

$$\rho_{\alpha\beta}(t) = \frac{i(f_\alpha - f_\beta) e v_F \boldsymbol{\sigma}_{\alpha\beta} \cdot \mathbf{E}}{\hbar\omega_l (\omega_l - \omega_{\alpha\beta} + i\gamma_{\alpha\beta})} e^{-i\omega_l t} \quad (\text{D3})$$

$$\equiv \rho_{\alpha\beta}(\omega_l) e^{-i\omega_l t}. \quad (\text{D4})$$

Note that the term

$$\frac{e v_F}{i\omega_l} \boldsymbol{\sigma}_{\alpha\beta} \cdot \mathbf{E} e^{-i\omega_l t} = \langle \alpha | H^{opt} | \beta \rangle;$$

the equality holds when we drop the complex conjugate part of H^{opt} . The right-hand side of the equation above

was calculated in Eq. (A9). We extract the following terms from Eq. (A9) for the Pauli matrix elements defined in Eq. (A8):

$$\sigma_{\alpha\beta}^+ = \langle \alpha | \sigma^+ | \beta \rangle = C_n C_m \delta_{k,k'} \sqrt{2} \text{sgn}(m) \delta_{|n|, |m|-1} \quad (\text{D5})$$

$$\sigma_{\alpha\beta}^- = \langle \alpha | \sigma^- | \beta \rangle = C_n C_m \delta_{k,k'} \sqrt{2} \text{sgn}(n) \delta_{|n|-1, |m|}. \quad (\text{D6})$$

The optical conductivity of graphene can be obtained from the expectation value of the 2D current density $\langle \mathbf{j}(t) \rangle$.

$$\begin{aligned} \langle \mathbf{j}(t) \rangle &= \text{tr}(\rho(-\frac{e}{S} \mathbf{v})) = -\frac{e}{S} \sum_{\alpha} \sum_{\beta} \rho_{\alpha\beta}(t) \mathbf{v}_{\beta\alpha} \\ &= -\frac{e}{S} \sum_{\alpha} \sum_{\beta} \rho_{\alpha\beta}(t) v_F \boldsymbol{\sigma}_{\beta\alpha} \end{aligned} \quad (\text{D7})$$

$$\begin{aligned} \langle \mathbf{j}(t) \rangle &= -i \frac{e^2 v_F^2}{S \hbar \omega_l} \sum_{\alpha} \sum_{\beta} \frac{(f_\alpha - f_\beta) (\boldsymbol{\sigma}_{\alpha\beta} \cdot \mathbf{E}) \boldsymbol{\sigma}_{\beta\alpha}}{(\omega_l - \omega_{\alpha\beta} + i\gamma_{\alpha\beta})} e^{-i\omega_l t} \\ &= \langle \mathbf{j}(\omega_l) e^{-i\omega_l t} \rangle. \end{aligned} \quad (\text{D8})$$

$$= \langle \mathbf{j}(\omega_l) e^{-i\omega_l t} \rangle. \quad (\text{D9})$$

In the component form

$$\langle j^p(\omega_l) \rangle = -i \frac{e^2 v_F^2}{S \hbar \omega_l} \sum_{r \neq p} \sum_{\alpha} \sum_{\beta} \frac{(f_\alpha - f_\beta) \sigma_{\beta\alpha}^p \sigma_{\alpha\beta}^r}{(\omega_l - \omega_{\alpha\beta} + i\gamma_{\alpha\beta})} E_p \quad (\text{D10})$$

$$\equiv \sum_{r \neq p} \sigma_{con}^{pr}(\omega_l) E_p, \quad (\text{D11})$$

where the indices p and r span over $+, -$.

There are four components of the conductivity tensor that we need to calculate: σ_{con}^{++} , σ_{con}^{--} , σ_{con}^{+-} , and σ_{con}^{-+} . The first two of them are equal to zero. The only nonzero elements are

$$\begin{aligned} \sigma_{con}^{+-}(\omega_l) &= -i \frac{e^2 v_F^2}{S \hbar \omega_l} \sum_{\alpha} \sum_{\beta} \frac{(f_\alpha - f_\beta) \sigma_{\beta\alpha}^+ \sigma_{\alpha\beta}^-}{(\omega_l - \omega_{\alpha\beta} + i\gamma_{\alpha\beta})} \\ &= -\frac{ie^2 v_F^2}{\hbar \omega_l} \frac{1}{\pi l_B^2} \sum_m \frac{f_{|m|+1} - f_m}{\omega_l - \omega_{|m|+1, m} + i\gamma_{|m|+1, m}}. \end{aligned} \quad (\text{D12})$$

$$\begin{aligned} \sigma_{con}^{-+}(\omega_l) &= -i \frac{e^2 v_F^2}{S \hbar \omega_l} \sum_{\alpha} \sum_{\beta} \frac{(f_\alpha - f_\beta) \sigma_{\beta\alpha}^- \sigma_{\alpha\beta}^+}{(\omega_l - \omega_{\alpha\beta} + i\gamma_{\alpha\beta})} \\ &= -\frac{ie^2 v_F^2}{\hbar \omega_l} \frac{1}{\pi l_B^2} \sum_m \frac{f_{|m|-1} - f_m}{\omega_l - \omega_{|m|-1, m} + i\gamma_{|m|-1, m}} \end{aligned} \quad (\text{D13})$$

σ_{con}^{+-} couples to the E_+ component of \mathbf{E} and σ_{con}^{-+} couples to the E_- component of \mathbf{E} . The TE-polarized pump fields in our problem are $\mathbf{E}^{1,2} = (\mathbf{E}_+^{(1,2)} + \mathbf{E}_-^{(1,2)}) e^{-i\omega_{1,2} t} + c.c.$. We also have $\omega_{|m|+1, -|m|}$ resonant with ω_1 and $\omega_{|m|-1, -|m|}$ resonant with ω_2 . For definiteness let's assume the initial state is $m = -3$ so ω_1 is resonant with $\omega_{4,-3}$ and ω_2 with $\omega_{2,-3}$. If we select only the resonant frequency then the conductivity becomes:

$$\sigma_{con}^{+-}(\omega_1) = -\frac{ie^2 v_F^2}{\hbar \omega_1} \frac{1}{\pi l_B^2} \frac{f_4 - f_{-3}}{\omega_1 - \omega_{4,-3} + i\gamma_{4,-3}} \quad (\text{D14})$$

where we expect $f_4 = 0$ and $f_{-3} = 1$. Note that $\sigma^{+-}(\omega_1)$ couples to $E_+^{(1)}$.

Similarly,

$$\sigma_{con}^{-+}(\omega_2) = -\frac{ie^2v_F^2}{\hbar\omega_2} \frac{1}{\pi l_B^2} \frac{f_2 - f_{-3}}{\omega_2 - \omega_{2,-3} + i\gamma_{2,-3}}, \quad (D15)$$

where we expect $f_2 - f_{-3} \simeq 0$ since both states are below the Fermi level.

-
- [1] A.H. Castro Neto, F. Guinea, N.M.R. Peres, K.S. Novoselov and A.K. Geim, *Rev. Mod. Phys.* 81, 110 (2009).
- [2] A.N. Grigorenko, M. Polini, and K.S. Novoselov, *Nat. Photonics* 6, 749 (2012).
- [3] Y.V. Bludov, A. Ferreira, N.M.R. Peres, and M.I. Vasilevskiy, *International Journal of Modern Physics B* 27, 1341001 (2013).
- [4] F. Rana, *Nanotechnology*, *IEEE Transactions on* 7, 91 (2008).
- [5] M. Jablan, H. Buljan, and M. Soljacic, *Phys. Rev. B* 80, 245435 (2009)
- [6] F.H.L. Koppens, D.E. Chang, and F.J. Garcia de Abajo, *Nano Lett.* 11, 3370 (2011).
- [7] M.F. Craciun, S. Russo, M. Yamamoto, and S. Tarucha, *Nano Today* 6, 42 (2011).
- [5] S. A. Mikhailov, *Phys. Rev. B* 79, 241309(R) (2009).
- [6] D.S.L. Abergel and V. I. Fal'ko, *Phys. Rev. B* 75, 155430 (2007).
- [10] E. Hendry, P.J. Hale, J. Moger, A.K. Savchenko, and S.A. Mikhailov, *PRL* 105, 097401 (2010).
- [11] X. Yao and A. Belyanin, *PRL* 108, 255503 (2012).
- [12] X. Yao, M.D. Tokman, and A. Belyanin, *Phys. Rev. Lett.* 112, 055501 (2014).
- [13] Y. Wang, M. Tokman, and A. Belyanin, *Phys. Rev. B* 94, 195442 (2016).
- [14] R.W. Boyd, *Nonlinear Optics*. 3rd ed. USA: Academic Press (an imprint of Elsevier), p. 28 (2008).
- [15] S.A. Mikhailov, *Phys. Rev. B* 84, 045432 (2011).
- [16] M. Tokman, Y. Wang, I. Oladyshkin, A. Ryan Kuttayah, and A. Belyanin, *Phys. Rev. B* 93, 235422 (2016).
- [17] J. L. Cheng, N. Vermeulen, and J. E. Sipe, *Sci. Rep.* DOI: 10.1038/srep43843 (2017).
- [18] B. Yao et al., *Nature Photonics* 12, 22 (2017).
- [19] K. Jamalpoor, A. Zarifkar, M. Miri, *Photonics and Nanostructures - Fundamentals and Applications* 26, 80 (2017).
- [20] J. Cao, Y. Kong, S. Gao, C. Liu, *Optics Comm.* 406, 183 (2018).
- [21] M. O. Goerbig, *Rev. Mod. Phys.* 83, 1193 (2011).
- [22] X. Yao and A. Belyanin, *J. Phys.: Condens. Matter* 25, 054203 (2013).
- [23] G. Giovannetti, P. A. Khomyakov, G. Brocks, P. J. Kelly, and J. van den Brink, *Phys. Rev. B* 76, 073103 (2007).
- [24] R. Decker, Y. Wang, V. W. Brar, W. Regan, H.-Z. Tsai, Q. Wu, W. Gannett, A. Zettl, and M. F. Crommie, *Nano Lett.* 11, 2291 (2011).
- [25] W. Yang, G. Chen, Z. Shi, Cheng-Cheng Liu, L. Zhang, G. Xie, M. Cheng, D. Wang, R. Yang, D. Shi, K. Watanabe, T. Taniguchi, Y. Yao, Y. Zhang and G. Zhang, *Nano Mat.* 12, 792 (2013).
- [26] C. H. Yang, F. M. Peeters, and W. Xu, *Phys. Rev. B* 82, 205428 (2010).
- [27] H. Funk, A. Knorr, F. Wendler, and E. Malic, *Phys. Rev. B* 92, 205428 (2015).
- [28] Y. Wang, M. Tokman, and A. Belyanin, *Phys. Rev. A* 91, 033821 (2015).
- [29] S. Brem, F. Wendler, and E. Malic, *Phys. Rev. B* 96, 045427 (2017).
- [30] M. Tokman, X. Yao, and A. Belyanin, *Phys. Rev. Lett.* 110, 077404 (2013).
- [31] P.A.D. Goncalves, and N.M.R. Peres, *An Introduction to Graphene Plasmonics*. 1st ed. Singapore: World Scientific Publishing Co. Pte. Ltd., p.17. (2016).
- [32] Y. Zheng and T. Ando, *Phys. Rev. B* 65, 245420 (2002).
- [33] J.W. McClure, *Phys. Rev.* 104, 666 (1956).
- [34] L.G. Booshehri, C.M. Mielke, D.G. Rickel, S.A. Cooker, Q. Zhang, L. Ren, E.H. Hazor, A. Rustagi, C.J. Stanton, Z. Jin, Z. Sun, Z. Yan, J.M. Tour, and J. Kono, *Phys. Rev. B* 85, 205407 (2012).
- [35] M.L. Sadowski, G. Martinez, M. Potemski, C. Berger, and W.A. de Heer, *Phys. Rev. Lett.* 97, 266405 (2006)
- [36] D.S.L. Abergel and V.I. Fal'ko, *Phys. Rev. B* 75, 155430 (2007).
- [37] Y. Wang, M. Tokman, and A. Belyanin, *Phys. Rev. A* 91, 033821 (2015).
- [38] J.P. Lu, *Phys. Rev. Lett.* 79, 1297 (1997).